

Identification and validation of a gray matter volume network in Alzheimer's disease

Munkhzaya Chuluunbat^{a,1}, Daiki Matsuda^{b,1}, Koji Fujita^{a,*}, Maki Otomo^c, Yoichi Otomi^c, Kohsuke Kudo^d, Masafumi Harada^c, Yushin Izumi^a

^a Department of Neurology, Tokushima University Graduate School of Biomedical Sciences, 3-18-15 Kuramoto-cho, Tokushima 770-8503, Japan

^b Tokushima University Faculty of Medicine, 3-18-15 Kuramoto-cho, Tokushima 770-8503, Japan

^c Department of Radiology and Radiation Oncology, Tokushima University Graduate School of Biomedical Sciences, 3-18-15 Kuramoto-cho, Tokushima 770-8503, Japan

^d Department of Diagnostic Imaging, Hokkaido University Faculty of Medicine, N15 W7 Kita-ku, Sapporo, Hokkaido 060-8638, Japan

ARTICLE INFO

Keywords:

Alzheimer's disease
Hippocampus
Multivariate analysis
Principal component analysis
Scaled subprofile model
Voxel-based morphometry

ABSTRACT

Objective: This study aims to identify and validate a gray matter volume network in patients with Alzheimer's disease (AD).

Methods: To identify a disease-related network, a principal component analysis-based algorithm, Scaled Subprofile Model, was applied to gray matter volume data derived from structural T1-weighted magnetic resonance imaging of the training sample that consisted of nine patients with AD (women, four; dementia, seven; mild cognitive impairment, two; age, 66.7 ± 8.8 [mean \pm SD] years) with positive ¹⁸F-flutemetamol amyloid positron emission tomography and eight age-matched healthy controls obtained on-site. The network expression scores were calculated by topographic profile rating in the validation sample obtained via the Open Access Series of Imaging Studies and comprised 12 patients with AD dementia (women, four; age, 70.0 ± 3.7 years) and 12 age-matched healthy controls.

Results: A significant network from the training sample, for which subject expression differed between the groups (permutation test, $P = 0.006$; sensitivity and specificity, 100%; area under the curve, 1), was identified. This network was represented by the principal components 1, 2, and 3 and showed a relative decrease in the inferior parietal lobule including angular gyrus, inferior temporal gyrus, premotor cortex, amygdala, hippocampus, and precuneus. It significantly differed between the groups with a sensitivity, specificity, and area under the curve of 83%, 91%, and 0.85, respectively, in the validation sample ($P = 0.003$).

Conclusions: An AD-related gray matter volume network that captured relevant regions was identified in amyloid positron emission tomography-positive patients and validated in an independent sample.

1. Introduction

Alzheimer's disease (AD) is the main cause of dementia and is rapidly becoming one of the most expensive, lethal, and burdening diseases worldwide [1]. The importance of accurate AD diagnosis is being increasingly recognized because it allows for the implementation of disease-modifying therapies in clinical settings. A research framework for AD diagnosis proposes to categorize individuals based on biomarker evidence of pathology using the so-called amyloid, tau, and neurodegeneration (ATN) classification system [2]. Four of the seven ATN

biomarkers are imaging-based: amyloid positron emission tomography (PET), tau PET, atrophy on structural magnetic resonance imaging (MRI), and hypometabolism on ¹⁸F-fluorodeoxyglucose PET. Of these, structural MRI has been a first line test for AD, demonstrating changes in the gray matter of the brain. Structural MRI findings in AD include both generalized and focal atrophy [3]. The most characteristic focal findings on MRI are hippocampal or medial temporal lobe atrophy. Of all the MRI AD markers, hippocampal atrophy assessed by high-resolution T1-weighted MRI is the best established and validated [3]. However, hippocampal atrophy can lack the sensitivity for early-onset AD variants

* Corresponding author.

E-mail address: kfujita@tokushima-u.ac.jp (K. Fujita).

¹ These authors contributed equally to this work.

Table 1
Profiles of patients with Alzheimer's disease in the training sample.

Age (years)	Sex	Diagnosis	MMSE	MOCA-J	Cortical motor sensory features*
58	M	AD dementia	20	15	ND
67	M	AD dementia	11	7	Ideomotor apraxia of right hand
77	F	MCI due to AD	19	14	ND
62	M	AD dementia	8	6	ND
78	F	MCI due to AD	21	17	ND
75	F	AD dementia	18	10	Ideomotor apraxia of bilateral hands
52	F	AD dementia	17	19	Ideomotor apraxia of bilateral hands
66	M	AD dementia	23	18	ND
65	M	AD dementia	17	17	ND

AD Alzheimer's disease, F female, M male, MCI mild cognitive impairment, MMSE Mini Mental State Examination, MOCA-J Japanese version of the Montreal Cognitive Assessment, ND not documented. *Limb apraxia, alien limb phenomenon, or cortical sensory loss or dyscalculia, which are included in diagnostic criteria for corticobasal syndrome [15].

with hippocampal sparing and focal parietal and other neocortical involvement. Moreover, medial temporal lobe or hippocampal atrophy lacks the specificity to exclude other dementias such as hippocampal sclerosis [4], argyrophilic grain disease [5], and primary age-related tauopathy [6]. These findings suggest that atrophy in other regions, such as the parietal lobe, should also be considered. However, differences in the shape and neuroanatomical configuration of individual brains may cause overlooking of structural alteration by visual inspection [7]. Moreover, visual inspection is inappropriate for the quantitative evaluation of regional brain volume changes [8].

Voxel-based morphometry (VBM) is a computational approach that can evaluate the local concentrations of brain tissue through voxel-wise analysis of brain images [7]. VBM can be used as a biomarker that predicts clinical disease progression and plays an important role in understanding AD pathology [9]. The VBM approach is unbiased to any structures and provides an even-handed and comprehensive assessment of anatomical differences throughout the brain [7]. That said, typical VBM methods with univariate analysis assess differences between patients and controls in isolated brain regions and can provide only local information but not an interregional covarying relationship of gray matter volumes among different brain regions.

In contrast, multivariate analysis can capture network-level changes in the brain. Scaled Subprofile Modelling/principal component analysis (SSM/PCA) is a multivariate method that allows the identification of disease-specific cerebral functional or structural networks [10]. A previous study [11] used SSM/PCA to analyze structural MRI data in AD patients, but the generalizability of the findings remains unaddressed. Therefore, the current study aimed to identify and validate a reliable, reproducible AD-related volume network.

2. Methods

2.1. Participants

Data from Tokushima University Hospital (TU) and the Open Series of Imaging Studies, Longitudinal MRI Data in Nondemented and Demented Older Adults (OASIS2) [12] were used for training and validation, respectively. The TU training sample comprised nine patients with AD (four females; age, 66.7 ± 8.8 [mean \pm standard deviation] years, range 52–78; Mini Mental State Examination [MMSE], $17.1 \pm$

4.8, range 8–23; Japanese version of the Montreal Cognitive Assessment [MoCA-J], 13.7 ± 4.9 , range 7–19), including three patients with early-onset AD (Table 1), and eight age- and sex-matched healthy controls (HCs; six females; age, 67.9 ± 9.2 years, range 55–82; MMSE, 28.6 ± 1.4 , range 26–30; MoCA-J, 26.3 ± 2.8 , range 23–30). The nine patients with AD showed positive amyloid PET scans, and of these, seven were diagnosed with probable AD dementia and two with mild cognitive impairment (MCI) due to AD as per the National Institute on Aging–Alzheimer's Association criteria [13,14]. The OASIS2 validation sample comprised 12 patients with AD dementia (four females; age, 70 ± 3.7 years, range 61–73; MMSE, 21.4 ± 4.4 , range 16–30; Clinical Dementia Rating, 1) and 12 age-matched HCs (nine females; age, 69.0 ± 5.9 years, range 60–79; MMSE, 29.3 ± 0.9 , range 27–30; Clinical Dementia Rating, 0). In OASIS2, the AD diagnosis was based on clinical information that the subject had experienced gradual onset and progression of decline in memory and other cognitive and functional domains [12]. The MMSE scores of patients with AD were lower in the TU training sample than in the OASIS2 validation sample (difference, 4.3; $P = 0.047$, *t*-test). This study was approved by the Ethics Committee of Tokushima University Hospital. Informed consent was obtained from all the participants of Tokushima University Hospital.

2.2. Image acquisition

TU data were obtained in a multicenter study from January 2018 to March 2019. 3D T1-weighted structural MRI was scanned using the Rf-Spoiled Steady state Gradient echo sequence with 3 Tesla TRILLIUM OVAL (Fujifilm, Tokyo, Japan). The parameters were repetition time 9.2 ms, echo time 4.3 ms, inversion time 1 s, flip angle 8° , acquisition matrix 256×256 , voxel size $0.938 \times 0.938 \times 0.7 \text{ mm}^3$, and slice thickness 1.4 mm. Amyloid PET was obtained as a 30-min scan 90 min after injection of $185.0 \pm 2.0 \text{ MBq } ^{18}\text{F}$ -flutemetamol (Vizamyl, GE Healthcare, Chicago, IL, USA) [16]. A nuclear medicine specialist (YO) trained to interpret ^{18}F -flutemetamol amyloid PET evaluated the images. OASIS2 MRI data scanned with 1.5 Tesla Vision (Siemens, Munich, Germany) [12] were obtained via <https://www.oasis-brains.org>.

2.3. Preprocessing

VBM techniques [7] were used in Statistical Parametric Mapping version 12 (SPM12; The Wellcome Centre for Human Neuroimaging, UCL Queen Square Institute of Neurology, London, UK; <https://www.fil.ion.ucl.ac.uk/spm/software/spm12/>) run with MATLAB R2019a (The MathWorks, Inc., Natick, MA, USA). First, 3D T1-weighted MRI was separated into gray and white matter images based on voxel intensities, and only gray matter images were used for normalization of the original images. Second, Diffeomorphic Anatomical Registration Through Exponentiated Lie Algebra (DARTEL) was used to improve the alignment accuracy between subjects [17]. Third, the images were spatially normalized to the Montreal Neurological Institute (MNI) space. Fourth, the normalized segments of each subject's gray matter image were modulated for gray matter volume analysis. Finally, all the images were smoothed with a Gaussian kernel of $8 \times 8 \times 8 \text{ mm}^3$ full width at the half maximum.

2.4. Network analysis

The SSM [10,18] was performed using the Generalized Covariance Analysis platform, version 1.2 (Columbia University Medical Center, NY, USA; www.nitrc.org/projects/gcva-pca), run in MATLAB and SPM. The preprocessed gray matter images of both the patients with AD and the HCs of the TU training sample were used for network identification. A gray matter mask was made applying the Masking toolbox (<http://www0.cs.ucl.ac.uk/staff/g.ridgway/masking/>) [19] to MRI data obtained via The Center for Biomedical Research Excellence (http://fcon_1000.projects.nitrc.org/indi/retro/cobre.html). The mean

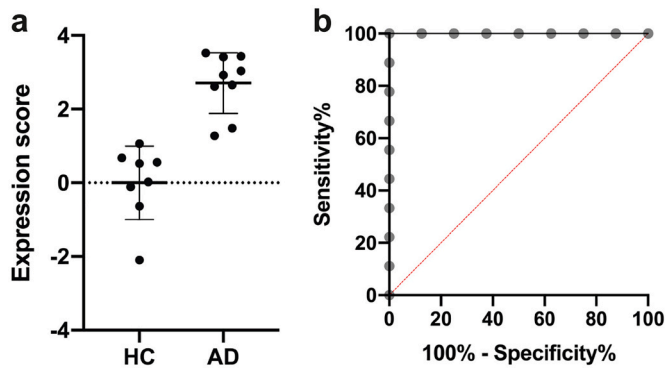


Fig. 1. Differentiation of Alzheimer's disease (AD) and healthy control (HC) using the expression of the AD-related gray matter network in the training data. **a** The expression scores were significantly higher in AD than HC. Error bars mean \pm SD. **b** The receiver operating characteristic curve of discriminability from the covariance pattern expression.

effects were subtracted from both the rows and columns of the subject \times voxel data matrix. PCA produced a set of principal components (PCs) along with the fraction of the variance by each PC. This operation also generated subject scores reflecting the degree to which a subject expressed the associated topography in each PC. A subset of top five PCs corresponding to an approximate cumulative variance of 50% [18] was examined to obtain a relevant topography. A set of PCs that yielded the lowest value in Akaike's information criterion was selected [20]. The selected PCs were then combined into a single PC vector. The optimal coefficients for the linear combination of the selected subject scores were determined by logistic regression of the corresponding subject scores using JMP 14 (SAS Institute Inc., Cary, NC). A produced covariance pattern was transformed to a z-score map standardized by the standard deviation. The subject scores were computed using the topographic profile rating and differences in the subject scores between the groups were evaluated using permutation tests (RStudio, Boston, MA) in the training

sample. A receiver operating characteristic (ROC) curve was used to identify sensitivity, specificity, and the area under the curve (AUC).

The voxels had a threshold of $Z = 1.64$ and were then examined and used for determining the related brain regions involved in the covariance network. The reliability of the voxel weights that significantly differed from zero was estimated using a bootstrapping algorithm. The PCA procedure was repeated for 1000 iterations by resampling the original sets of gray matter images with replacements, and a voxel map of the inverse coefficient of variation (ICV) was produced. The significance level for voxel weight reliability was set at an ICV threshold of $Z = 1.64$ corresponding to $P < 0.05$ [21].

The covariance pattern derived from the training sample was prospectively applied to the preprocessed gray matter scans of the OASIS2 validation sample to test the pattern expression.

3. Results

Via the spatial covariance analysis of the gray matter images obtained from the combined group of nine patients with AD and eight HCs, we identified a significant pattern with differing subject expression between the two groups ($P = 0.006$, permutation test). This pattern was represented by a linear combination of PCs 1, 2, and 3 (coefficients, 0.73, 0.33, and 0.59, respectively), which accounted for 14.9% of the overall subject \times voxel variance. ROC curve analysis exhibited discrimination with a sensitivity of 100% (95% confidence interval [CI], 70.0–100), specificity of 100% (95%CI, 67.6–100), and AUC of 1 ($P < 0.001$) in the training data (Fig. 1). The network, termed AD-related gray matter network, was characterized by a relative reduction in the inferior parietal lobule including angular gyrus, inferior temporal gyrus, premotor cortex, amygdala, hippocampus, and precuneus (Fig. 2 and Table 2). In patients with AD, the subject scores of the network did not correlate with the MMSE scores ($r = -0.157$ [95%CI, -0.744 – 0.566], $P = 0.687$, Pearson correlation coefficient); In contrast, higher network expression tended to be associated with lower MoCA-J scores ($r = -0.641$ [95%CI, -0.915 – 0.04], $P = 0.063$, Pearson correlation coefficient).

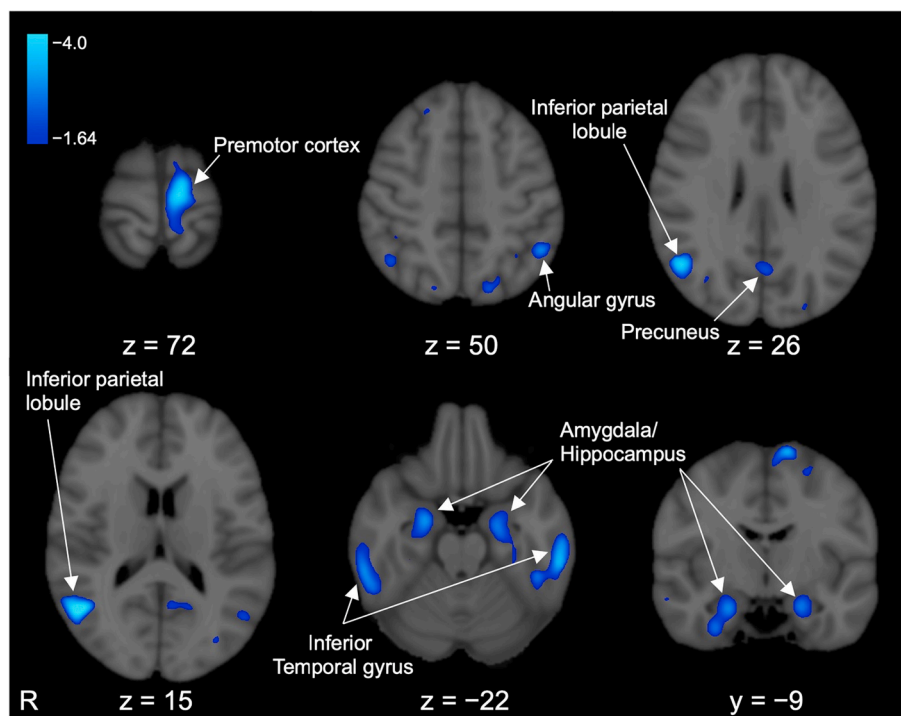


Fig. 2. Alzheimer's disease-related gray matter volume network obtained in the training sample. Negative weights represent relative decrease in patients with Alzheimer's disease compared with healthy controls.

Table 2
Regions characterizing the Alzheimer's disease-related gray matter network.

Brain regions	Peak MNI coordinates (x, y, z; mm)			Voxels	Z max
Decrease					
R Inferior parietal lobule	51	-60	15	6642	4.41
L Inferior temporal gyrus	-58.5	-30	-22.5	3838	3.58
L Premotor cortex	-10	-18	72	2220	4.02
R Amygdala, hippocampus	22.5	-4.5	-24	2156	3.32
L Amygdala, hippocampus	-21	-9	-22.5	1324	2.92
L Inferior parietal lobule (angular gyrus)	-48	-51	49.5	1177	3.11
L Precuneus cortex	-1.5	-63	25.5	981	2.44
R Superior frontal gyrus	21	16.5	60	686	4.29
L Superior parietal lobule	-18	-72	54	584	3.13
R Cingulate gyrus, posterior division	6	-33	42	314	2.11
L Superior frontal gyrus	-24	-3	57	290	2.93
L Lateral occipital cortex	-31.5	-76.5	19.5	267	3.15
R Lateral occipital cortex	33	-78	19.5	255	2.47
R Supramarginal gyrus	39	-43.5	45	162	2.46
L Superior frontal gyrus	-21	25.5	54	151	2.47
R Middle frontal gyrus	34.5	34.5	39	150	2.5
L Superior parietal lobule	-33	-51	45	143	2.33
L Lateral occipital cortex	-31.5	-88.5	-6	105	2.42
Increase					
L Cerebellum VI lobule	-31.5	-49.5	-31.5	6313	3.32
L Paracingulate gyrus	12	52.5	0	1002	2.69
L Frontal pole	-34.5	55.5	-4.5	845	2.72
L Occipital pole	-13.5	-102	12	511	2.17
R Paracingulate gyrus	-10.5	55.5	7.5	359	2.33
R Precentral gyrus	60	7.5	21	353	2.25
L Occipital pole	0	-93	-15	329	2.87
L Cerebellum VIIIb lobule	-13.5	-60	-51	263	2.02
L Heschl's gyrus	-48	-25.5	6	245	2.33
R Occipital pole	18	-99	-6	195	2.02
R Paracingulate gyrus	9	42	22.5	154	2.03
L Cingulate gyrus, anterior division	-6	39	18	105	2.07

Brain region labels were determined following the Harvard–Oxford cortical structural atlas, Jülich histological (cyto- and myelo-architectonic) atlas, and cerebellar atlas in FSLeyes as part of the FMRIB Software Library (FSL) version 6.0 (Analysis Group, FMRIB, Oxford, UK; <https://fsl.fmrib.ox.ac.uk/fsl/fslwiki/FSL>). The clusters had a threshold of $Z = 1.64$ ($P < 0.05$). Furthermore, bootstrap estimation demonstrated the reliability of the voxel weights ($|\text{inverse coefficient of variation}| > 1.64$). Clusters with >100 voxels were reported. *L* left, *MNI* Montreal Neurological Institute, *R* right.

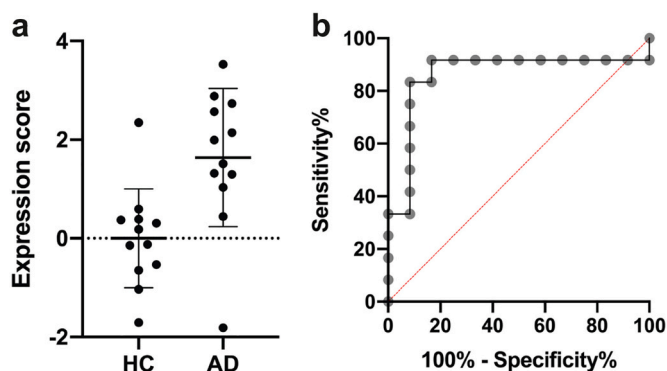


Fig. 3. Differentiation of Alzheimer's disease (AD) and healthy control (HC) by expression of the AD-related gray matter network in the validation data. **a** The expression scores were significantly higher in AD than HC. *Error bars* mean \pm SD. **b** The receiver operating characteristic curve of discriminability from the covariance pattern expression.

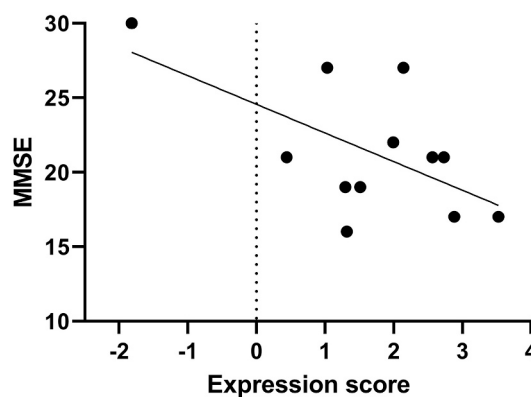


Fig. 4. Correlation of network expression and Mini Mental State Examination (MMSE) in patients with Alzheimer's disease in the validation sample ($r = -0.605$, $P = 0.037$, Pearson correlation coefficient).

In the OASIS2 validation sample, the subject scores of the AD-related covariance pattern were also significantly higher in patients with AD than the HCs ($P = 0.003$, *t*-test). ROC curve analysis showed an AUC of 0.861 (95%CI, 0.684–1, $P = 0.003$). A cut-off value with the highest likelihood ratio discriminated AD from HC with a sensitivity of 83.3% (95%CI, 55.2–97.0) and specificity of 91.7% (95%CI, 64.6–99.6) (Fig. 3). The subject scores of the network significantly correlated with the MMSE scores of the patients with AD ($r = -0.605$ [95%CI, -0.875 – -0.048], $P = 0.037$, Pearson correlation coefficient) (Fig. 4).

4. Discussion

An AD-related network covariance pattern using two independent datasets acquired by different MRI scans and from different ethnic groups was identified and validated in the current study. The SSM/PCA applied to the training sample, in which the AD diagnosis required positive amyloid PET, identified the AD-related gray matter network. Expression scores of the pattern were significantly higher in AD patients than HC in both training and validation samples. Similarly, the ROC curve analyses demonstrated discrimination with reasonably high sensitivity and specificity in both the training and validation samples. These findings suggest that the SSM/PCA with VBM technique can reliably differentiate AD from healthy condition regardless of MRI machine or patient ethnicity.

The AD-related gray matter network comprises the inferior parietal lobule including angular gyrus, inferior temporal gyrus, premotor cortex, amygdala, hippocampus, and precuneus as the relatively decreased regions. Structural changes measured by VBM have been independently reported in these regions in patients with AD. First, decrease in gray matter volume in the inferior parietal lobule and angular gyrus, which is essential for processes relating to spatial cognition [22], was associated with conversion from MCI to AD dementia [23]. Second, volume reduction in the inferior temporal gyrus has been associated with AD and amnesic MCI [24]. Third, gray matter volume in the premotor cortex has been shown to be reduced in AD with corticobasal syndrome [25], although it is relatively preserved in AD with typical amnesic syndrome. Patients with AD in our training sample presented with amnesic syndrome but some also had ideomotor apraxia, which may be associated with frontal and parietal cortices including premotor cortex [26], and could have affected the relative reduction in the premotor cortex in the gray matter network. Fourth, the medial temporal lobe, including the amygdala and hippocampus, is especially vulnerable in patients with AD. Hence, the amygdalar and hippocampal volume loss has been reported in patients with AD [27,28]. A meta-analysis depicted that volume reduction in the left hippocampus and parahippocampal gyrus is a marker of conversion from amnesic MCI to AD dementia [29]. Fifth, early-onset AD was associated with lesser gray matter volume in

the precuneus, which was independent from hippocampal atrophy, and a smaller precuneus has been associated with impaired visuospatial functioning [30]. We note the hippocampus and precuneus are clusters of the default mode network [31], where hypometabolism on ^{18}F -fluorodeoxyglucose PET has been observed in patients with AD [32,33]. Resting-state functional MRI studies have demonstrated that functional connectivity between the hippocampus and precuneus is reduced in patients with AD [34]. It is noteworthy that the network we have identified and validated in the present study has incorporated these relevant brain regions in a single pattern with high reproducibility.

Compared with previous studies, the current study has several advantages. First, AD diagnosis was supported by the presence of amyloid β as revealed by amyloid PET in the training sample, which could reduce variance unrelated with AD. Second, contrary to a previous study whose training and validation samples employed MRI data obtained in the same country and with the same type of scanners [11], the training and validation samples of the current study were obtained from different ethnic profiles and using different scanner types and magnetic field strengths, thus broadening the generalizability of the findings. Third, we examined only top five PCs to reduce overfitting. In contrast, the pattern in the previous study included as many as 10 PCs, exhibiting a sensitivity of 84% and specificity of 90% in the training sample and only a sensitivity of 69% and specificity of 71% in the validation sample, indicating that the model was overfitting. Fourth, we were able to derive and validate a significant network in patients with relatively mild impairment compared with the previous study where the mean MMSE was 11.7 (range 0–23) in the training sample and 18.5 (range 12–23) in the validation sample. Fifth, we found a significant, albeit modest, correlation between network expression and cognitive function in the validation sample.

This study has several limitations. First, the number of participants was small. Data should be expanded in the future to render these findings more robust. Second, the images of patients with preclinical AD were not evaluated. Third, the differential diagnosis of other dementing disorders was outside the scope of the current study.

In conclusion, the current study demonstrated a gray matter network covariance pattern that could reproducibly distinguish between patients with AD and healthy subjects. This multivariate analysis could be applied to the clinical field to improve AD diagnosis.

Funding

This research was partly supported by AMED under Grant Number JP18he1402002.

Data availability statement

The data that support the findings of this study are available from the corresponding author upon reasonable request.

Acknowledgements

Data were provided in part by OASIS: Longitudinal: Principal Investigators: D. Marcus, R. Buckner, J. Csernansky, J. Morris; P50 AG05681, P01 AG03991, P01 AG026276, R01 AG021910, P20 MH071616, U24 RR021382. The authors would like to thank Enago (www.enago.jp) for the English language review.

References

- [1] P. Scheltens, B. De Strooper, M. Kivipelto, et al., Alzheimer's disease, *Lancet* 397 (2021) 1577–1590, [https://doi.org/10.1016/S0140-6736\(20\)32205-4](https://doi.org/10.1016/S0140-6736(20)32205-4).
- [2] C.R. Jack Jr., D.A. Bennett, K. Blennow, et al., NIA-AA research framework: toward a biological definition of Alzheimer's disease, *Alzheimers Dement.* 14 (2018) 535–562, <https://doi.org/10.1016/j.jalz.2018.02.018>.
- [3] G.B. Frisoni, N.C. Fox, C.R. Jack Jr., P. Scheltens, P.M. Thompson, The clinical use of structural MRI in Alzheimer disease, *Nat. Rev. Neurol.* 6 (2010) 67–77, <https://doi.org/10.1038/nrneuro.2009.215>.
- [4] D.C. Woodworth, H.L. Nguyen, Z. Khan, et al., Utility of MRI in the identification of hippocampal sclerosis of aging, *Alzheimers Dement.* 17 (2021) 847–855, <https://doi.org/10.1002/alz.12241>.
- [5] K. Sakurai, A.M. Tokumaru, T. Ikeda, et al., Characteristic asymmetric limbic and anterior temporal atrophy in demented patients with pathologically confirmed argyrophilic grain disease, *Neuroradiology* 61 (2019) 1239–1249, <https://doi.org/10.1007/s00234-019-02247-4>.
- [6] M. Quintas-Neves, M.A. Teylan, L. Besser, et al., Magnetic resonance imaging brain atrophy assessment in primary age-related tauopathy (PART), *Acta Neuropathol. Commun.* 7 (2019) 204, <https://doi.org/10.1186/s40478-019-0842-z>.
- [7] J. Ashburner, K.J. Friston, Voxel-based morphometry—the methods, *Neuroimage* 11 (2000) 805–821, <https://doi.org/10.1006/nimg.2000.0582>.
- [8] H. Matsuda, E. Imabayashi, Structural neuroimaging in Alzheimer's disease, in: H. Matsuda, T. Asada, A.M. Tokumaru (Eds.), *Neuroimaging Diagnosis for Alzheimer's Disease and Other Dementias*, Springer Tokyo, Tokyo, 2017, pp. 21–38, <https://doi.org/10.1007/978-4-431-55133-1>.
- [9] P. Vemuri, C.R. Jack Jr., Role of structural MRI in Alzheimer's disease, *Alzheimers Res. Ther.* 2 (2010) 23, <https://doi.org/10.1186/alzrt47>.
- [10] P. Spetsieris, Y. Ma, S. Peng, et al., Identification of disease-related spatial covariance patterns using neuroimaging data, *J. Vis. Exp.* 76 (2013) 50319, <https://doi.org/10.3791/50319>.
- [11] X. Guo, K. Chen, Y. Zhang, Y. Wang, L. Yao, Regional covariance patterns of gray matter alterations in Alzheimer's disease and its replicability evaluation, *J. Magn. Reson. Imaging* 39 (2014) 143–149, <https://doi.org/10.1002/jmri.24143>.
- [12] D.S. Marcus, T.H. Wang, J. Parker, et al., Open access series of imaging studies (OASIS): cross-sectional MRI data in young, middle aged, nondemented, and demented older adults, *J. Cogn. Neurosci.* 19 (2007) 1498–1507, <https://doi.org/10.1162/jocn.2007.19.9.1498>.
- [13] G.M. McKhann, D.S. Knopman, H. Chertkow, et al., The diagnosis of dementia due to Alzheimer's disease: recommendations from the National Institute on Aging-Alzheimer's Association workgroups on diagnostic guidelines for Alzheimer's disease, *Alzheimers Dement.* 7 (2011) 263–269, <https://doi.org/10.1016/j.jalz.2011.03.005>.
- [14] M.S. Albert, S.T. DeKosky, D. Dickson, et al., The diagnosis of mild cognitive impairment due to Alzheimer's disease: recommendations from the National Institute on Aging-Alzheimer's Association workgroups on diagnostic guidelines for Alzheimer's disease, *Alzheimers Dement.* 7 (2011) 270–279, <https://doi.org/10.1016/j.jalz.2011.03.008>.
- [15] R. Mathew, T.H. Bak, J.R. Hodges, Diagnostic criteria for corticobasal syndrome: a comparative study, *J. Neurol. Neurosurg. Psychiatry* 83 (2012) 405–410, <https://doi.org/10.1136/jnnp-2011-300875>.
- [16] T. Otani, H. Otsuka, K. Matsushita, et al., Effect of different examination conditions on image quality and quantitative value of amyloid positron emission tomography using ^{18}F -flutemetamol, *Ann. Nucl. Med.* 35 (2021) 1004–1014, <https://doi.org/10.1007/s12149-021-01634-3>.
- [17] J. Ashburner, A fast diffeomorphic image registration algorithm, *Neuroimage* 38 (2007) 95–113, <https://doi.org/10.1016/j.neuroimage.2007.07.007>.
- [18] P.G. Spetsieris, D. Eidelberg, Scaled subprofile modeling of resting state imaging data in Parkinson's disease: methodological issues, *Neuroimage* 54 (2011) 2899–2914, <https://doi.org/10.1016/j.neuroimage.2010.10.025>.
- [19] G.R. Ridgway, R. Omar, S. Ourselin, D.L. Hill, J.D. Warren, N.C. Fox, Issues with threshold masking in voxel-based morphometry of atrophied brains, *Neuroimage* 44 (2009) 99–111, <https://doi.org/10.1016/j.neuroimage.2008.08.045>.
- [20] C. Habeck, N.L. Foster, R. Pernecky, et al., Multivariate and univariate neuroimaging biomarkers of Alzheimer's disease, *Neuroimage* 40 (2008) 1503–1515, <https://doi.org/10.1016/j.neuroimage.2008.01.056>.
- [21] C. Habeck, Y. Stern, Alzheimer's disease neuroimaging initiative, multivariate data analysis for neuroimaging data: overview and application to Alzheimer's disease, *Cell Biochem. Biophys.* 58 (2010) 53–67, <https://doi.org/10.1007/s12013-010-9093-0>.
- [22] H.I. Jacobs, M.P. Van Boxtel, J. Jolles, F.R. Verhey, H.B. Uylings, Parietal cortex matters in Alzheimer's disease: an overview of structural, functional and metabolic findings, *Neurosci. Biobehav. Rev.* 36 (2012) 297–309, <https://doi.org/10.1016/j.neubiorev.2011.06.009>.
- [23] G. Karas, J. Sluimer, R. Goekoop, Amnesic mild cognitive impairment: structural MR imaging findings predictive of conversion to Alzheimer disease, *Am. J. Neuroradiol.* 29 (2008) 944–949, <https://doi.org/10.3174/ajnr.A0949>.
- [24] G.F. Busatto, B.S. Diniz, M.V. Zanetti, Voxel-based morphometry in Alzheimer's disease, *Expert. Rev. Neurother.* 8 (2008) 1691–1702, <https://doi.org/10.1586/14737175.8.11.1691>.
- [25] K.A. Josephs, J.L. Whitwell, B.F. Boeve, Anatomical differences between CBS-corticobasal degeneration and CBS-Alzheimer's disease, *Mov. Disord.* 25 (2010) 1246–1252, <https://doi.org/10.1002/mds.23062>.
- [26] R.G. Gross, M. Grossman, Update on apraxia, *Curr. Neurol. Neurosci. Rep.* 8 (2008) 490–496, <https://doi.org/10.1007/s11910-008-0078-y>.
- [27] A. Shiino, T. Watanabe, K. Maeda, et al., Four subgroups of Alzheimer's disease based on patterns of atrophy using VBM and a unique pattern for early onset disease, *Neuroimage* 33 (2006) 17–26, <https://doi.org/10.1016/j.neuroimage.2006.06.010>.
- [28] X. Guo, Z. Wang, K. Li, et al., Voxel-based assessment of gray and white matter volumes in Alzheimer's disease, *Neurosci. Lett.* 468 (2010) 146–150, <https://doi.org/10.1016/j.neulet.2009.10.086>.

- [29] L.K. Ferreira, B.S. Diniz, O.V. Forlenza, et al., Neurostructural predictors of Alzheimer's disease: a meta-analysis of VBM studies, *Neurobiol. Aging* 32 (2011) 1733–1741, <https://doi.org/10.1016/j.neurobiolaging.2009.11.008>.
- [30] G. Karas, P. Scheltens, S. Rombouts, et al., Precuneus atrophy in early-onset Alzheimer's disease: a morphometric structural MRI study, *Neuroradiology* 49 (2007) 967–976, <https://doi.org/10.1007/s00234-007-0269-2>.
- [31] M.E. Raichle, The brain's default mode network, *Annu. Rev. Neurosci.* 38 (2015) 433–447, <https://doi.org/10.1146/annurev-neuro-071013-014030>.
- [32] T. Kato, Y. Inui, A. Nakamura, K. Ito, Brain fluorodeoxyglucose (FDG) PET in dementia, *Ageing Res. Rev.* 30 (2016) 73–84, <https://doi.org/10.1016/j.arr.2016.02.003>.
- [33] J.A. Maldjian, C.T. Whitlow, Alzheimer's disease neuroimaging initiative, whither the hippocampus? FDG-PET hippocampal hypometabolism in Alzheimer disease revisited, *Am. J. Neuroradiol.* 33 (2012) 1975–1982, <https://doi.org/10.3174/ajnr.A3113>.
- [34] G. Allen, H. Barnard, R. McColl, Reduced hippocampal functional connectivity in Alzheimer disease, *Arch. Neurol.* 64 (2007) 1482–1487, <https://doi.org/10.1001/archneur.64.10.1482>.